CONFERENCE PROCEEDINGS

Numerical Simulation of CO_2 Sequestration in Saline Aquifers with Geomechanical Effects

P. H. Winterfeld and Y. S. Wu, Colorado School of Mines, Golden, CO 80401

TENTH ANNUAL CONFERENCE ON CARBON CAPTURE AND SEQUESTRATION – May 2-5, 2011

Abstract

We developed a reservoir simulator for modeling CO_2 transport in saline aquifers coupled with geomechanical processes that would occur during CO_2 sequestration. These geomechanical processes, namely pressure and thermally induced rock deformation, affect rock permeability, porosity, and bulk volume. The theories of hydrostatic and linear poroelasticity and correlations from the literature are used to obtain dependencies of rock permeability, porosity, and bulk volume on pore pressure, stress, and temperature. These dependencies are incorporated into the simulator's mass and energy conservation equations, which determine pressure, temperature, and fluid composition. Stress is either assumed constant or varies with changes in aquifer mass distribution. The simulator is based on the TOUGH2-MP code (Zhang et al. 2008) with the ECO2N module (Pruess, 2005), which calculates properties of H_2O-NaCl-CO_2 mixtures. These mixtures consist of one aqueous and one CO_2-rich phase, salt can precipitate and dissolve in the aqueous phase, and the mixture temperature may change. The simulator is fully implicit, three-dimensional, the grid is unstructured, and the linear equations associated with the conservation equations are solved in porous and fractured media. The simulator code is parallelized and uses MPI for processor communication, the METIS software package for domain partitioning, and the Aztec solver package for linear equation solution.

The simulator is validated using example problems from the literature, and options for the above dependencies are also illustrated. One example problem (Birkholzer et al., 2008) is a study of the volume influenced during and after CO_2 injection into a saline aquifer. Another (Rutqvist and Tsang, 2002) addresses coupled hydromechanical changes during CO_2 injection into an aquifer–caprock system. In this example, geomechanical processes were modeled by coupling two simulators, TOUGH2 (Pruess et al., 1999), which simulates fluid flow and heat transport, and FLAC3D (FLAC3D, 1997), which simulates rock and soil mechanics with thermomechanical and hydromechanical interactions. Finally, the last example problem (Kumar et al., 2005) is a simulation of a prototypical CO_2 sequestration project in a deep saline aquifer using a commercially available simulator (Nghiem, 2001).

Introduction

Geological sequestration of CO_2 in deep saline aquifers is a primary option for reducing anthropogenic CO_2 emissions into the atmosphere. Deep saline aquifers are widely distributed, contain high salinity water that is unfit for human consumption, and can accommodate large volumes of CO_2. CO_2 is injected into these aquifers as a supercritical fluid with a liquid-type density and a gas-type viscosity. The critical point of CO_2, 31.1 °C and 7.4 MPa, corresponds to an aquifer depth of about 800 m. Sequestration is achieved by trapping supercritical CO_2 in the aquifer pore spaces (either as a separate phase trapped beneath impermeable rock or through capillary forces where CO_2 is an immobile phase), dissolution of CO_2 in the saline aqueous phase (which is dependent on pressure, temperature, and salinity), and reaction of CO_2 with minerals present in the rock. Reactions with minerals require a much longer time scale than the other sequestration mechanisms and are not considered in this paper.

Numerical simulation of CO_2 sequestration is an active research area. Two simulators that have been used extensively for CO_2 sequestration modeling are GEM™ (Ngheim et al., 2001) and the TOUGH2 family of codes (Pruess et al. 1999; Pruess, 2005; Zhang et al. 2007). These simulators model flow in porous media with convection and dispersion, and equilibrium between phases and components. Geomechanical effects are also important to consider in CO_2 sequestration simulation, because injection results in pressure increases and changes in reservoir stresses and strains that effect rock transport properties and could cause rock to fracture, allowing CO_2 to leak into the surroundings. Ngheim et al. (2004), Settari and Mourits (1998), and others have included geomechanical effects in those flow simulations by coupling a porous media flow simulator to a geomechanical one. In this coupling, the porous media and geomechanical models run concurrently and periodically exchange information common to both, such as porosity and volume, in order to calculate solutions that are consistent with one another.

In this paper, we take a different and simpler approach to including geomechanical effects in porous media flow simulations. Terzaghi, (1936) first introduced the concept of effective stress, the difference between average stress and pore pressure, during his studies of the mechanics of saturated soils. This

concept was further refined by Biot (1941) and others. Theories of poroelasticity (Geertsma, 1957; Carrol and Katsube, 1983; Zimmerman 1991) have related rock properties such as porosity to effective stress, and experimental studies (e.g., Nur and Byerlee, 1971) have supported these relations. The dependence of permeability on porosity has had numerous investigators (Bear, 1972) and an early example is the Carman-Kozeny hydraulic radius model. In addition, Gobran et al. (1987) concluded that permeability is dependent on the difference between confining pressure and pore pressure (effective stress) but not on their actual values. We incorporate geomechanical effects in the mass and energy balances of a conventional reservoir simulator by adding effective stress dependence of porosity and permeability, and related properties. These dependencies are obtained from theories of poroelasticity and empirical correlations from the literature. We also make the simplifying assumption of a time-invariant stress field.

TOUGH2 Simulators

Our simulator is a modification of TOUGH2-MP (Zhang et al. 2008), a massively parallel version of TOUGH2 (Pruess et al. 1999). TOUGH2 is a numerical simulator of multi-component, multiphase fluid and heat flow in porous and fractured media. TOUGH2 was designed primarily for applications in geothermal reservoir engineering, nuclear waste disposal, and environmental assessment and remediation. In the TOUGH2 formulation, fluid advection is described with a multiphase extension of Darcy's law and there is diffusive mass transport in all phases. Heat flow occurs by conduction and convection, and includes sensible as well as latent heat effects. Phases are in local equilibrium. TOUGH2 solves mass and energy balances over the simulation domain using the integral finite difference method (Narasimhan and Witherspoon, 1976) on an unstructured grid. The integral form of these balances is

$$\frac{d}{dt}\int M^k dV = \int \bar{F}^k \cdot \hat{n} d\Gamma + \int q^k dV \qquad (1)$$

where, for component k, M^k is mass in V, q^k is source or sink, $\bar{F}^k$is flux through Γ, the boundary of V, and $\hat{n}$ is the outward unit normal vector to Γ. Mass accumulation is a sum over phases

$$M^k = \phi \sum_j S_j \rho_j X_j^k \qquad (2)$$

where ϕ is porosity, S is phase saturation, ρ is mass density, and X is mass fraction of component k. Energy accumulation, M^{N+1}, is

$$M^{N+1} = (1-\phi) C_r \rho_r T + \phi \sum_j S_j \rho_j u_j \qquad (3)$$

where ρ_r is rock density, C_r is rock specific heat, T is temperature, and u is phase specific internal energy. The integral finite difference method replaces volume integrals with volume averages,

$$\int M^k dV = \overline{M^k} V \qquad (4)$$

and surface integrals with surface averages

$$\int \bar{F}^k \cdot \hat{n} d\Gamma = \sum_m A_m F_m^k \qquad (5)$$

Mass fluxes are summed over phases and have advective and diffusive portions. The time derivative in Equation 1 is replaced by a standard first order finite difference approximation, the fluxes are fully implicit, and the resulting set of nonlinear of algebraic equations shown below are solved using the Newton-Raphson method

$$R^{n+1} = M^{k,n+1} - M^{k,n} - \frac{\Delta t}{V}\left\{\sum_m A_m F_m^{k,n+1} + Vq^{k,n+1}\right\} = 0 \quad (6)$$

where n is time level.

TOUGH2 consists of functional units, such as a grid generator and a physical property module, with flexible and transparent interfaces. The physical property module is ECO2N (Pruess, 2005; Pruess and Spycher, 2007). ECO2N was designed for CO_2 sequestration in saline aquifers. It includes a description of the relevant properties of H_2O–NaCl–CO_2 mixtures that is highly accurate for the temperature, pressure, and salinity conditions of interest (between 10 and 110 °C, pressure less than 600 bar, and salinity up to full halite saturation). An aqueous and a CO_2-rich phase may be present, and salt may be present in the aqueous phase or as a solid precipitate. ECO2N can model super- as well as sub-critical conditions, but does not make the distinction between liquid and gaseous CO_2.

The highlights of TOUGH2-MP (Zhang et al. 2008), the massively parallel version of TOUGH2, are domain partitioning, and parallel assembly and solution of the Jacobian matrix. Domains are partitioned using the METIS package with three partitioning algorithm options, K-Way, VK-Way, and Recursive. Each processor computes Jacobian matrix elements for its own grid blocks. Exchange of information between processors allows calculation of Jacobian matrix elements associated with inter-block connections across domain partition boundaries. The Jacobian matrix is solved in parallel using an iterative linear solver from the Aztec package. Different solver options, such as conjugate gradient and generalized minimum residual, are available.

Rock Deformation Model

Our rock deformation model is based on the concept of effective stress. Effective stress was initially defined as the difference between average stress and pore pressure by Terzhagi (1936) and was generalized by Biot and Willis (1957) as

$$\sigma' = \sigma_m - \alpha P \quad (7)$$

where α is the Biot or effective stress coefficient. We approximate average stress as the overburden stress

$$\sigma_m = P_{atm} + \int_0^z \left((1-\phi)\rho_r + \phi\sum_p S_p\rho_p\right) g\,dz \quad (8)$$

or we input the spatial average stress distribution. Permeability and porosity are both dependent on effective stress

$$k = k(\sigma') \quad (9)$$

$$\phi = \phi(\sigma') \quad (10)$$

Since bulk volume is related to porosity, we also allow bulk volume to depend on effective stress and pore pressure

$$V_b = V_b(\sigma', P) \quad (11)$$

In addition, permeability and porosity are used to scale capillary pressure according to the relation by Leverett (1941)

$$P_c = P_{c0}\frac{\sqrt{(k/\phi)_0}}{\sqrt{(k/\phi)}} \quad (12)$$

where subscript 0 refers to reference conditions.

Property Correlations

A theory of hydrostatic poroelasticity (Zimmerman et al. 1986) has been proposed that accounts for the coupling of rock deformation with fluid flow inside the porous rock. Porous rock has a bulk and a pore volume, and those volumes are acted on by pore pressure and average stress. Four compressibilities are written in terms of those quantities, for example

$$C_{bc} = \frac{-1}{V_b}\left(\frac{\partial V_b}{\partial \sigma_m}\right)_P \tag{13}$$

where subscript b refers to bulk volume . Relationships between these compressibilities are derived for an idealized porous medium and from that, dependence of porosity on effective stress

$$d\phi = -[C_{bc}(1-\phi) - C_r]d\sigma' \tag{14}$$

where C_r is rock grain compressibility, an expression for the Biot coefficient

$$\alpha = 1 - \frac{C_r}{C_{bc}} \tag{15}$$

and dependence of bulk volume on pore pressure and effective stress

$$dV_b = -V_b C_{bc} d\sigma' + C_r dP \tag{16}$$

Rutqvist et al. (2002) presented the following function for porosity, obtained from laboratory experiments on sedimentary rock by Davies and Davies (1999)

$$\phi = \phi_r + (\phi_0 - \phi_r)e^{-a\sigma'} \tag{17}$$

where ϕ_0 is zero effective stress porosity, ϕ_r is high effective stress porosity, and the exponent a is a parameter. They also presented an associated function for permeability in terms of porosity

$$k = k_0 e^{c\left(\frac{\phi}{\phi_0}-1\right)} \tag{18}$$

where k_0 is zero stress permeability and the exponent c is a parameter. For fractured media, they defined an aperture width b_k for direction k as

$$b_k = b_{0,k} + \Delta b_k\left(e^{-d\sigma'} - e^{-d\sigma'_0}\right), k = x, y, z \tag{19}$$

where subscript 0 refers to initial conditions, Δb_k is the aperture change, and the exponent d is a parameter. Porosity is correlated to changes in b_k as

$$\phi = \phi_0 \frac{b_1+b_2+b_3}{b_{1,0}+b_{2,0}+b_{3,0}} \tag{20}$$

and direction k permeability is correlated to fracture aperture of other directions l and m as

$$k_k = k_{k,0}\frac{b_l^3+b_m^3}{b_{l,0}^3+b_{m,0}^3} \tag{21}$$

McKee et al. (1988) derived a relationship between porosity and effective stress from hydrostatic poroelasticity theory by assuming incompressible rock grains

$$\phi = \phi_0 \frac{e^{-c_p\left(\sigma' - \sigma_0'\right)}}{1-\phi_0\left(1-e^{-c_p\left(\sigma' - \sigma_0'\right)}\right)} \tag{22}$$

where c_p is average pore compressibility. A relationship between permeability and effective stress was obtained from the Carman-Kozeny equation

$$k \propto \frac{\phi^3}{(1-\phi)^2} \tag{23}$$

and the above relationship for porosity. These relationships fit laboratory and field data for granite, sandstone, clay, and coal.

Ostensen (1986) studied the relationship between effective stress and permeability for tight gas sands and approximated permeability as

$$k^n = D\ln\frac{\sigma'^{,*}}{\sigma'} \tag{24}$$

where n is 0.5, D is a parameter, and $\sigma'^{,*}$ is effective stress for zero permeability, obtained by extrapolating measured square root permeability versus effective stress on a semi-log plot.

Verma and Pruess (1988) presented a power law expression relating permeability to porosity

$$\frac{k-k_c}{k_0-k_c} = \left(\frac{\phi-\phi_c}{\phi_0-\phi_c}\right)^n \tag{25}$$

where k_c and ϕ_c are asymptotic values of permeability and porosity, respectively, and exponent n is a parameter.

The porosity correlations described in this section are summarized in Table 1 and the permeability correlations in Table 2.

Table 1: Porosity correlations

Option	Source	Equation
1	(Zimmerman, 1986) poroelasticity	14, 16*
2	Rutqvist et al. (2002), sedimentary rock	17
3	Rutqvist et al. (2002), fractures	20
4	McKee (1988)	22

* Equation for bulk volume change

Table 2: Permeability correlations

Option	Source	Equation
1	Rutqvist et al. (2002), sedimentary rock	18
2	Rutqvist et al. (2002), fractures	21
3	Carman-Kozeny	23
4	Ostensen (1986)	24
5	Verma and Pruess (1988)	25

Example Simulations and Discussion

We describe simulations of CO_2 injection into saline aquifers. In our first set of simulations, we illustrate some of the capabilities of our simulator and how rock deformation affects results. In our second set, we match some results from a coupled multiphase flow-rock deformation simulation. In our third set, we refine the grid of a published simulation to illustrate the capabilities of the parallel code to run large problems.

Birkholzer et al. (2008) studied the volume influenced during and after CO_2 injection into a saline aquifer. They were interested in determining how far pressure perturbations and brine migration caused by CO_2 injection extend beyond the CO_2 plume itself and whether these two can potentially interact with shallow groundwater resources nearby. They represented the saline aquifer as a two-dimensional radially symmetric volume that consists of alternating aquitard and aquifer layers with the bottom aquifer resting on impermeable rock. Each aquifer is 60 m thick, each aquitard is 100 m thick, and their radius is 200 km, intended to be large enough to minimize boundary effects. Fluid can escape through the radial boundary, which is maintained at hydrostatic pressure. CO_2 is injected into the bottom aquifer at 1.52 million tonnes per year for 30 years, followed by a 70-year post injection period. Temperature varies linearly from 15 °C at the surface to 38.6 °C at the bottom, and salinity varies with elevation as well. Additional details are given in the reference.

We use this example to illustrate some of the capabilities of our simulator and how rock deformation affects results, and we simulate only the bottom aquitard-aquifer pair of their system. We reran their base case, which has constant aquifer and aquitard permeability (10^{-13} m^2 and 10^{-18} m^2, respectively) and pore compressibilities (4.5×10^{-10} Pa^{-1} and 9.0×10^{-10} Pa^{-1}, respectively) on a 200×50 grid. Figure 1 shows the CO_2 saturation profile after 30 years of injection. This profile agrees with their published results. CO_2 is restricted to the bottom aquifer with a small amount entering the above low permeability aquitard. We then reran this simulation with our effective stress-dependent permeability and porosity options and used Equation 8 for the average stress. The first run used Porosity Option 2 from Table 1 and constant permeability. The high stress porosity in Equation 17 is ten percent less than the initial (0.20 for the aquifer and 0.05 for the aquitard), from which zero stress values are calculated. The exponential parameters are 4.5×10^{-8} Pa^{-1} and 9.0×10^{-8} Pa^{-1} for the aquifer and aquitard, respectively. Figure 2 shows percent increase of porosity after 30 years of injection. The aquitard has a somewhat higher porosity increase than the aquifer, but the aquifer porosity increase is more developed axially. The aquifer is envisioned to be sandstone and the aquitard shale. Sandstone is more permeable and less compressible than shale, as reflected by their input properties. The greater aquitard compressibility allows for a greater porosity percent increase than in the aquifer, but the greater aquifer permeability results in more developed axial profiles. Our second run used Porosity Option 4 from Table 1 and constant permeability. The average pore compressibility in Equation 22 is equal to the base case. Figure 3 shows the percent increase of porosity. Overall, the porosity increase was small and the aquitard percent increase was again greater than the aquifer. In this run, the porosity versus effective stress relationship is that for a slightly compressible medium, and porosity increase is small. In the first run, that relationship was obtained from a fit of laboratory data on sandstone compression. Sandstone compression involves rearrangement, as

well as compression, of individual rock grains. The result of including this additional mechanism of porosity change was a larger porosity increase.

We ran three additional cases with Porosity Option 2 from Table 1 and Permeability Options 1, 3, and 5 from Table 2. For Permeability Option 1, the exponent c was 22.2 (from Rutqvist et al., 2002). Permeability Option 3 requires no parameters and for Permeability Option 5, the exponent n was 1.4, k_c/k_o was 0.45, and ϕ_c/ϕ_o was 0.9 (from Verma and Pruess, 1988). Figures 4-6 show the percent permeability increase after 30 years of CO_2 injection for the respective permeability options. Figure 4 shows the most sensitivity to increasing porosity, Figure 6 shows an intermediate amount, and Figure 5 shows the least. One effect of permeability increasing with porosity is decreasing pressure buildup in the vicinity of the injector. Figures 7 and 8 show pressure buildup at 30 years injection for the base case (no permeability increase) and the Porosity Option 2, Permeability Option 1 case. Rock fracturing during CO_2 sequestration is undesirable since fractures could provide an avenue of escape for CO_2 trapped under caprock. The lower pressure buildup predicted from including these geomechanical effects would allow for a higher injection rate than otherwise.

Rutqvist and Tsang (2002) simulated CO_2 injection into a hypothetical aquifer-caprock system covered by semi-permeable shale. They coupled two computer codes, TOUGH2 for multiphase flow and heat transport, and FLAC3D (FLAC3D, 1997) for rock deformation, to study the hydraulic, mechanical, and hydromechanical changes during injection including the spread of the CO_2 plume, effective stress and permeability changes, and ground surface uplift. The two codes were coupled through correlating porosity as a function of effective stress and permeability as a function of porosity, which are our Porosity Option 2 and Permeability Option 2. FLAC3D calculates stress tensor components in the simulation volume and effective stress is calculated using the mean of the normal stress components.

The aquifer is 200 m thick and is bounded above by 100 m thick caprock. Above the caprock is a homogeneous formation that extends to the surface and below the aquifer is also caprock. The aquifer properties are that of sandstone and the caprock's are that of shale. The system is two-dimensional and effectively infinite in lateral extent. We ran their simulation using Porosity Option 1 and Permeability Option 1 on a 201x100 grid. The injector was located at the aquifer bottom and lateral midpoint, and CO_2 was injected at 0.05 kg/sec for 30 years. Bulk volume compressibility in Equation 14 was 5.5×10^{-10} Pa^{-1} for the aquifer and 5.0×10^{-11} Pa^{-1} for the caprock, rock grain compressibility was zero, and other input properties can be found in the reference. The CO_2 plume at 1, 3, and 10 years are shown in Figures 9-11, respectively. These agree well with the reference, shown in Figure 12. Porosity Option 1 includes bulk volume change. This was used to calculate ground surface uplift by assuming uniform volume change in all directions. Figure 13 shows this uplift at 1, 3, and 10 years and Figure 14 shows the reference results. Both are very similar. Figure 15 shows the permeability changes at 10 years. Most of the permeability changes are in the vicinity of the injector. In the reference, permeability changes are there and along the upper and lower aquifer-caprock interfaces, shown in Figure 16. We were not able to match permeability change there since our calculations assume constant stress. Figure 17 compares injection block pressure for this simulation with one without rock deformation (constant porosity and permeability). Again, inclusion of rock deformation results in lower pressure buildup.

Kumar et al. (2005) simulated a hypothetical CO_2 injection project into a deep saline aquifer to better understand and quantify CO_2 storage mechanisms. They studied the impact of parameters such as permeability, residual gas saturation, salinity, and temperature on CO_2 storage. Their base case was an aquifer 304.8 m thick and 16,154 m in length and width, with a one degree dip. Porosity was 0.25, temperature was 60 °C, and there were ten horizontal strata of varying permeability with the lower half being greater than the upper. 27.6 kg/sec CO_2 was injected for fifty years in a well located at the areal center and perforated along the lower half of the reservoir, followed by thousands of years of equilibration. Constant pressure wells were situated along the boundaries to model an open aquifer. The reference contains additional details.

We ran their base case with a finer grid to demonstrate the parallel code's ability to run larger simulations. We used a Dell PC with eight Intel® Xeon® E5405 2.0 GHz processors with total memory of 15.7 GB, and a Linux operating system. Our grid was 100x100x100, with 1,000,000 active grid blocks. We ran 50 years of CO_2 injection followed by 1,000 years of equilibration; the simulation took about 65 hours. Figure 18 shows CO_2 saturation at 50 years for a cross section containing the injector. The CO_2 plume is fairly symmetric except for the higher permeability layers where it already is moving

up dip (towards smaller x-values). Figure 19 shows CO_2 saturation at 1,000 years for the same cross section. The up dip CO_2 migration is more pronounced, the CO_2 saturation profile is more diffuse, and there is CO_2 accumulation in the lower permeability zone above the bottom five perforated ones.

Summary and Conclusions

We developed a massively parallel reservoir simulator based on the TOUGH2-MP code with the ECO2N module for modeling CO_2 flow and transport in saline aquifers coupled with geomechanics. We incorporated into the simulator mass and energy conservation equations dependencies of rock permeability, porosity, and bulk volume on pore pressure and average stress, obtained from the theories of hydrostatic and linear poroelasticity and correlations from the literature.

We verified the simulator formulation, numerical implementation, and computational efficiency using example problems from the literature. We used a study of CO_2 injection into a saline aquifer to compare results from various porosity and permeability dependencies on effective stress, and found that they differ based on the physical assumptions behind the porosity and permeability dependencies. We compared our results to those from two coupled computer codes, one that simulates fluid flow and heat transport, and another that simulates rock deformation. We obtained a good match of the CO_2 plume and surface uplift at various times, indicating that our formulation is able to capture effects modeled by the more rigorous coupled simulation, but noted limitations on the permeability match. We reran a simulation on a finer grid, illustrating the parallel code's ability to run larger problems.

Nomenclature

A = area, m^2
b_i = i-direction fracture aperture, m
C = compressibility, Pa^{-1}
g = gravitational acceleration, m/sec^2
k = permeability, m^2
F = component mass flux, kg/sec
M = component mass, kg
P = pore pressure, Pa
P_{atm}=atmospheric pressure, Pa
P_c = capillary pressure, Pa
q = component generation, kg/sec
S = phase saturation
T = temperature, °K
u = phase specific internal energy, J/kg
V = volume, m^3
X = phase mass fraction
α =biot coefficient
Γ = surface area, m^2
ρ = density, kg/m^3
σ_m= mean stress, Pa
σ'= effective, stress, Pa
ϕ = porosity

Acknowledgements

This work was supported by the Assistant Secretary for Fossil Energy, Office of Coal and Power R&D through the National Energy Technology Laboratory under U.S. Department of Energy Contract Number DE-FC26-09FE0000988.

References

Bear, J.: “Dynamics of Fluids in Porous Materials”, Elsevier, New York, 1972.

Biot, M.A.: “General Theory of Three-Dimensional Consolidation,” J. Appl. Phys., 12, 155-164, 1941.

Biot, M.A. and Willis, D.G.: “The Elastic Coefficients of the Theory of Consolidation,” J. Appl. Mech., 24, 594–601, 1957

Birkholzer, J.T., Zhou, Q., Tsang, C.-F.: “Large-Scale Impact of CO2 Storage in Deep Saline Aquifers: A Sensitivity Study on Pressure Response in Stratified Systems,” Int. J. Greenhouse Gas Control 3, 181-194, 2008.

Carroll, M.M. and Katsube, N.: “The Role of the Terzaghi Stress in Linearly Elastic Deformation,” ASME J. Energy Res. Technol., 105, 509-511, 1983.

Davies J.P. and Davies D.K.: “Stress-Dependent Permeability: Characterization and Modeling,” Society of Petroleum Engineers, SPE 56813, 1999.

FLAC3D, Manual: “Fast Lagrangian Analysis of Continua in 3 Dimensions-Version 2.0.,” Itasca Consulting Group Inc, Minnesota, 1997.

Geertsma, J.: “The Effect of Fluid Pressure Decline on Volumetric Changes of Porous Rock,” Trans. AIME, 210,331-339, 1957.

Gobran B. D., Brigham W. E., and Ramey H.J. Jr.: “Absolute Permeability as a Function of Confining Pressure, Pore Pressure, and Temperature,” SPE Formation Evaluation, 77-84, 1987

Kumar, A., Ozah, R. , Noh, M. , Pope, G.A. , Bryant, S. , Sepehrnoori, K. , and Lake, L.W. : “Reservoir Simulation of CO2 Storage in Deep Saline Aquifers,” Soc. Pet. Eng. J., 10(3), 336 – 348, 2005.

Leverett, M.C.: “Capillary Behavior in Porous Media,” Trans. AIME, 142:341–58, 1041.

McKee, C.R., Bumb, A.C., and Koenig, R.A.: “Stress-Dependent Permeability and Porosity of Coal and Other Geologic Formations,” SPE Formation Evaluation, 81, March 1988.

Narashimhan T. N. and Witherspoon, P. A.: “An Integrated Finite Difference Method for Analysis of Fluid Flow in Porous Media,” Water Resour Res 1976;12:57–64.

Nghiem, L.X., Kohse, B.F., Sammon, P.H., “Compositional Simulation of the VAPEX Process,” J. Can. Pet. Technol. 40 (8), 54–61, 2001.

Nghiem, L., Sammon, P., Grabenstetter, J. and Ohkuma, H.: “Modeling CO2 Storage in Aquifers with a Fully-Coupled Geochemical EOS Compositional Simulator,” Proceedings 2004 SPE/DOE Fourteenth Symposium on Improved Oil Recovery Tulsa, Oklahoma, U.S.A., 17–21 April 2004.

Nur, A. and Byerlee, J.D.: “An Exact Effective Stress Law for Elastic Deformation of Rock with Fluids,” J Geophys Res 76, 6414-9, 1971.

Ostensen, R.W.: “The Effect of Stress-Dependent Permeability on Gas Production and Well Testing,” SPE 11220, SPE Form. Eval., pp. 227–235, June 1986.

Pruess K. and Spycher. N.: “ECO2N – A Fluid Property Module for the TOUGH2 Code for Studies of CO2 Storage in Saline Aquifers,” Energy Conversion and Management, 48, 1761-1767, 2007.

Pruess, K.: “ECO2N: A TOUGH2 Fluid Property Module for Mixtures of Water, NaCl, and CO_2,” Research Report, LBNL-57952, Lawrence Berkeley National Laboratory, Berkeley, CA, 2005.

Pruess K, Oldenburg C, Moridis G.: “TOUGH2 User’s Guide, Version 2.0,” Report LBNL-43134, Berkeley, California: Lawrence Berkeley National Laboratory, 1999.

Rutqvist, J., and Tsang, C.F.: “A Study of Caprock Hydromechanical Changes Associated with CO2-Injection into a Brine Formation,” Environ. Geol. 42, 296–305, 2002.

Rutqvist J, Wu YS, Tsang C-F, and Bodvarsson G.: “A Modeling Approach for Analysis of Coupled Multiphase Fluid Flow, Heat Transfer, and Deformation in Fractured Porous Rock,” Int J Rock Mech Min Sci, 39, 429–42, 2002.

Settari, A. and Mourits, F.M.: “A Coupled Reservoir and Geomechanical Modeling System,” SPEJ, 219. September 1998.

Terzaghi, K.: “The Shearing Resistance of Saturated Soils and the Angle Between the Planes of Shear,” Proceedings of International Conference on Soil Mechanics and Foundation Engineering, vol. 1, pp. 54-56, Harvard University Press, Cambridge, Mass., 1936

Verma, A., and Pruess, K.: “Thermohydrological Conditions and Silica Redistribution Near High-Level Nuclear Wastes Emplaced in Saturated Geological Formations. J. Geophys. Res., 93, 1159-1173, 1988.

Zhang, K., Wu, Y.S., and Pruess.M K.: “User’s Guide for TOUGH2-MP - A Massively Parallel Version of the TOUGH2 Code,” LBNL-315E, Earth Sciences Division, Lawrence Berkeley National Laboratory, May, 2008.

Zhang, K., Doughty, C., Wu, Y.S., and Pruess, K.: “An Efficient Parallel Simulation of CO_2 Geologic Sequestration in Saline Aquifers, paper SPE-106026, 2007 SPE Reservoir Simulation Symposium, Houston TX, Feb. 26-28, 2007.

Zimmerman, R.W.: “Compressibility of Sandstones,” Amsterdam, Elsevier, 1991.

Zimmerman, R.W., Somerton,W. H., and King, M.S.: “Compressibility of Porous Rocks,” J. Geophys. Res 91, 12, 765–77, 1986.

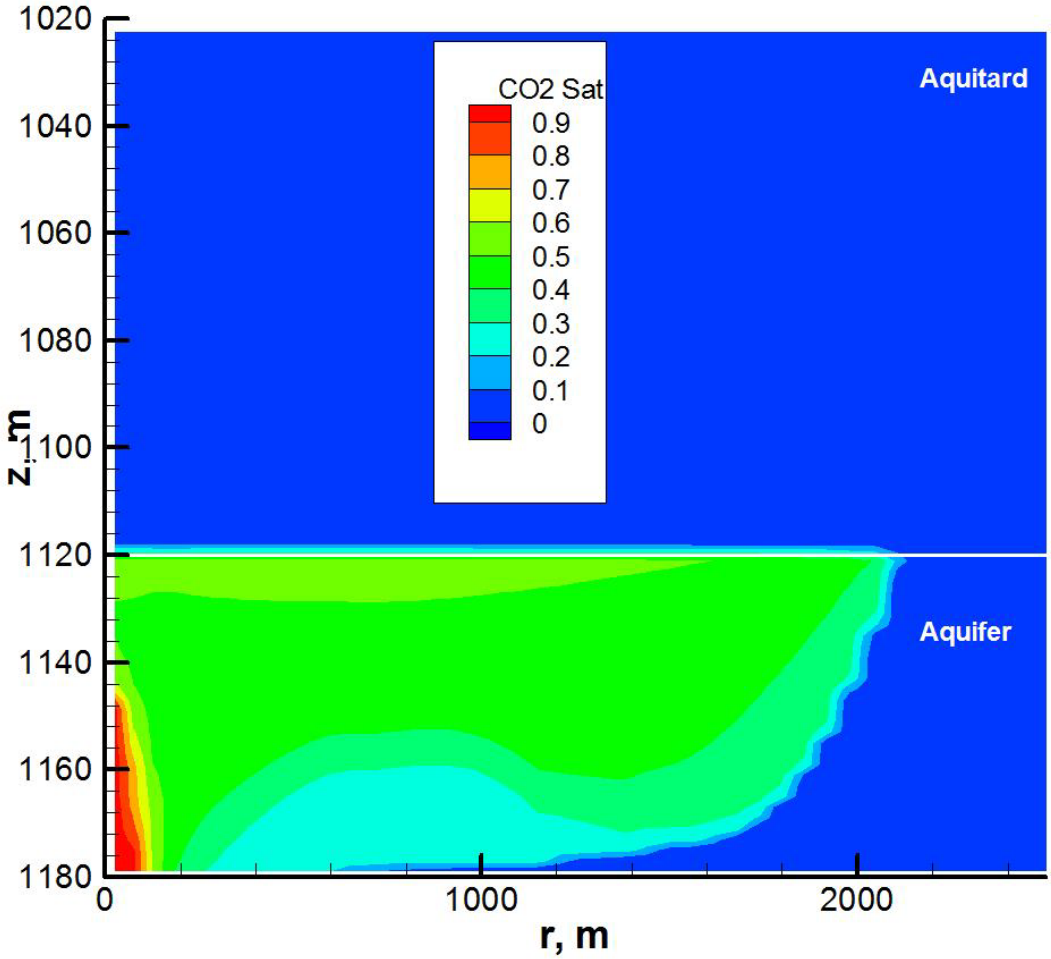

Figure 1: CO_2 saturation for modified Birkholzer et al. (2008) simulation base case with compressible pores and constant permeability.

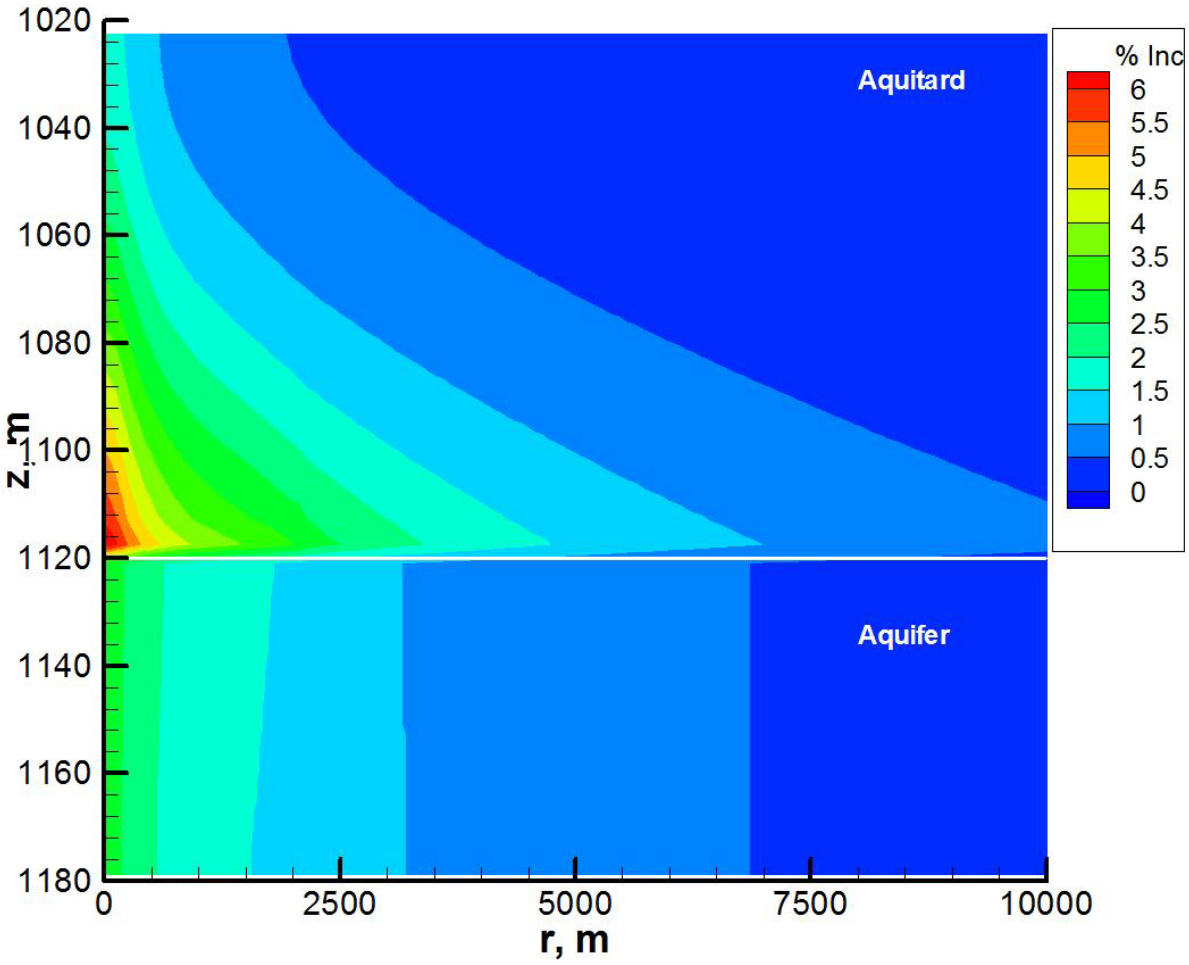

Figure 2: Percent increase of porosity after 30 years of injection; modified Birkholzer et al. (2008) simulation with Porosity Option 2 from Table 1 and constant permeability.

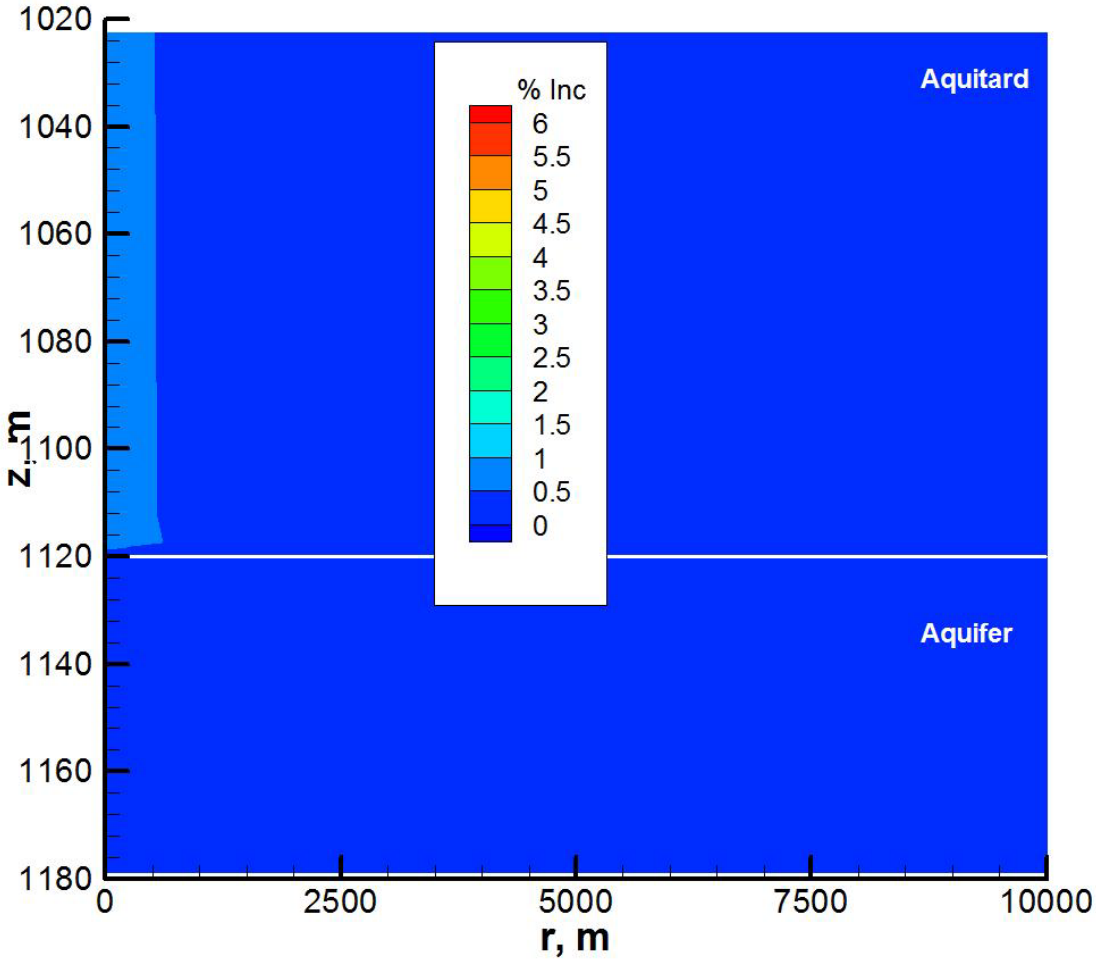

Figure 3: Percent increase of porosity after 30 years of injection; modified Birkholzer et al. (2008) simulation with Porosity Option 4 from Table 1 and constant permeability.

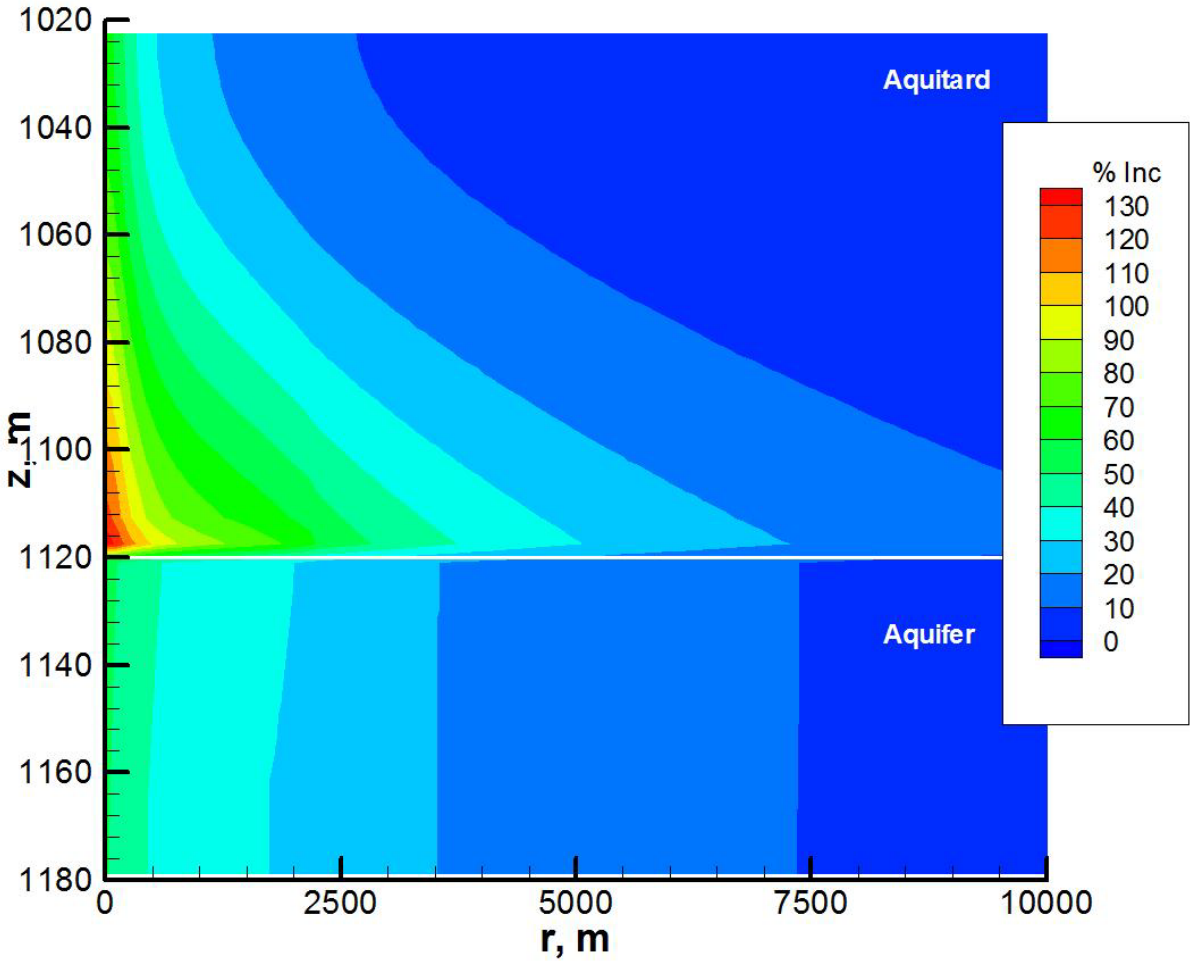

Figure 4: Percent increase of permeability after 30 years of injection; modified Birkholzer et al. (2008) simulation with Porosity Option 4 from Table 1 and Permeability Option 1 from Table 2.

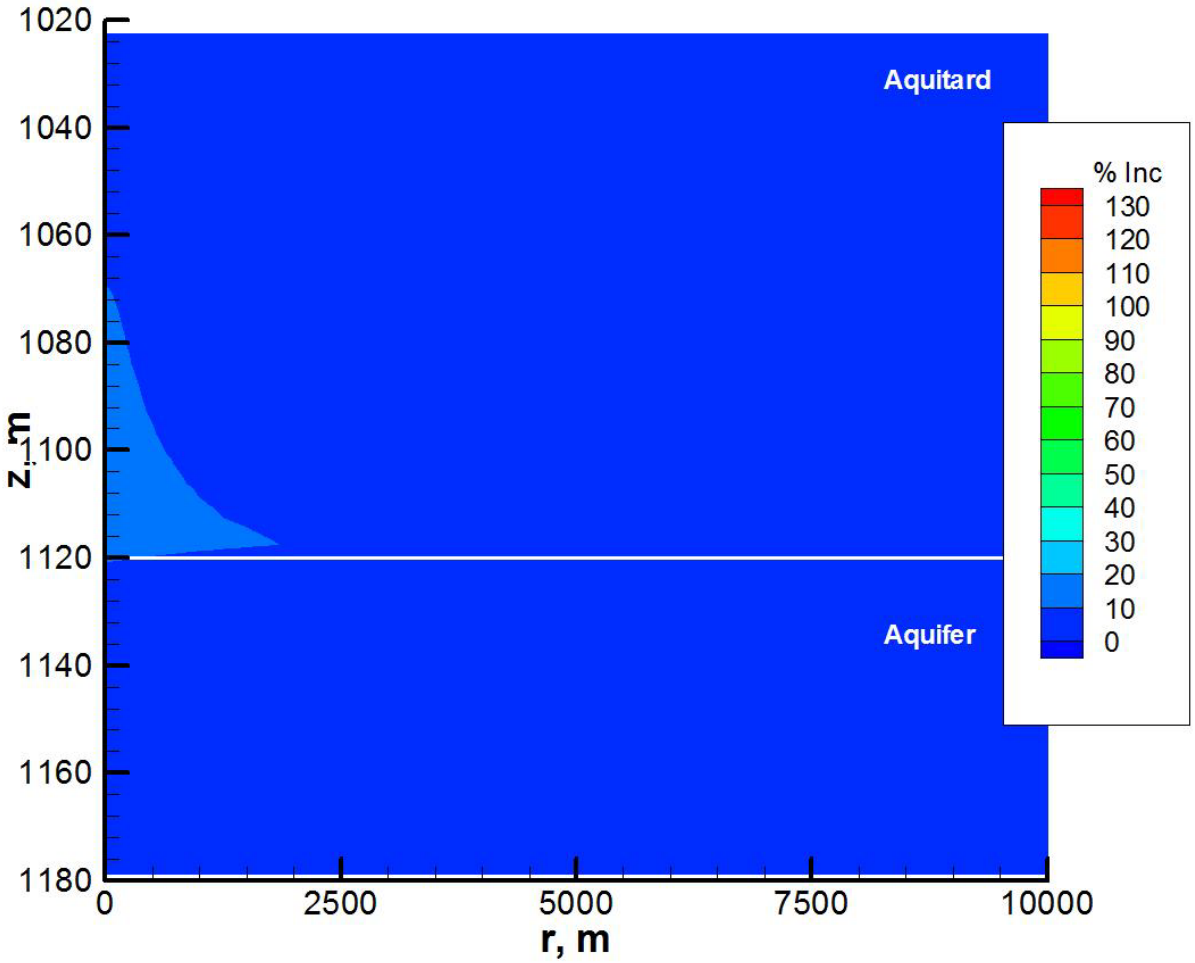

Figure 5: Percent increase of permeability after 30 years of injection; modified Birkholzer et al. (2008) simulation with Porosity Option 4 from Table 1 and Permeability Option 3 from Table 2.

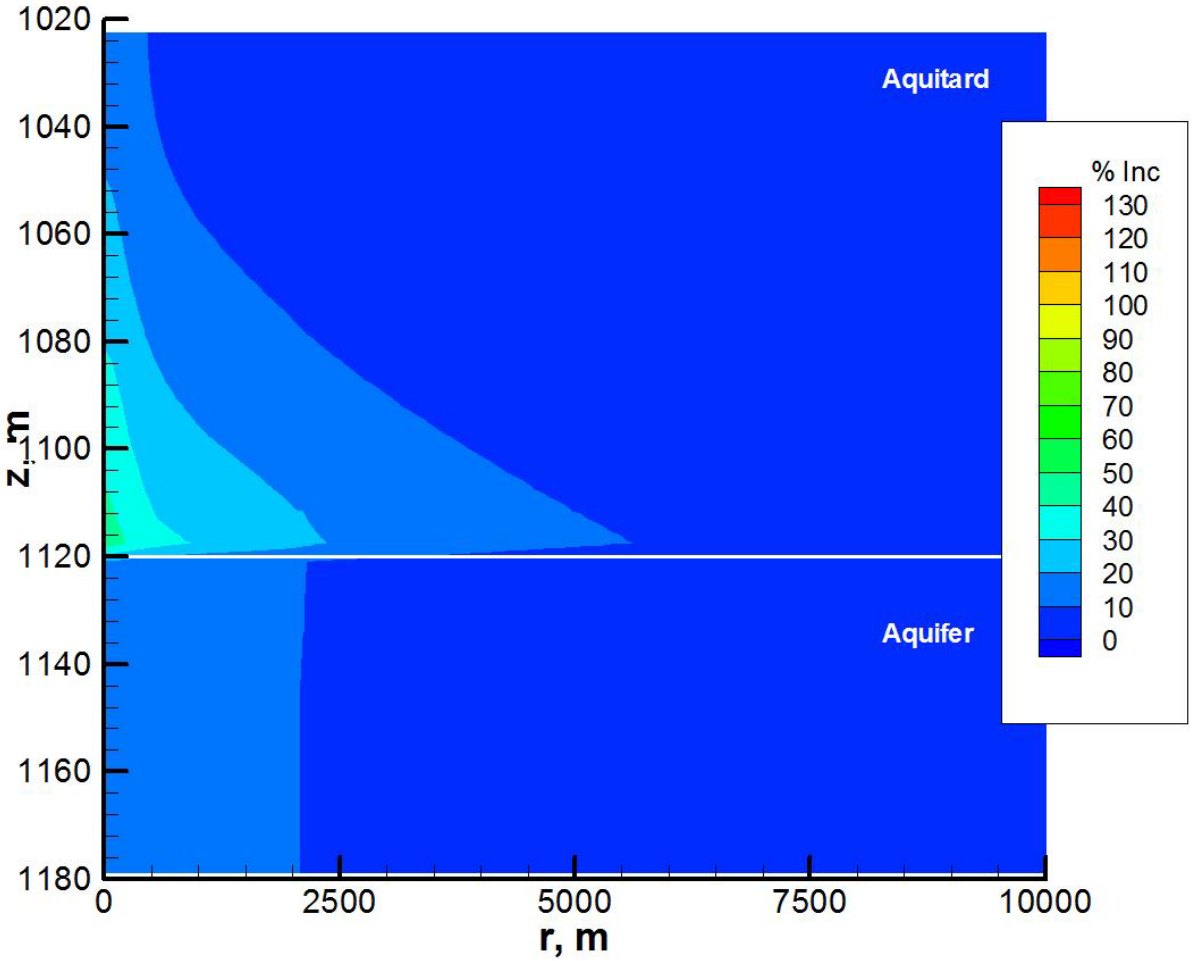

Figure 6: Percent increase of permeability after 30 years of injection; modified Birkholzer et al. (2008) simulation with Porosity Option 4 from Table 1 and Permeability Option 5 from Table 2.

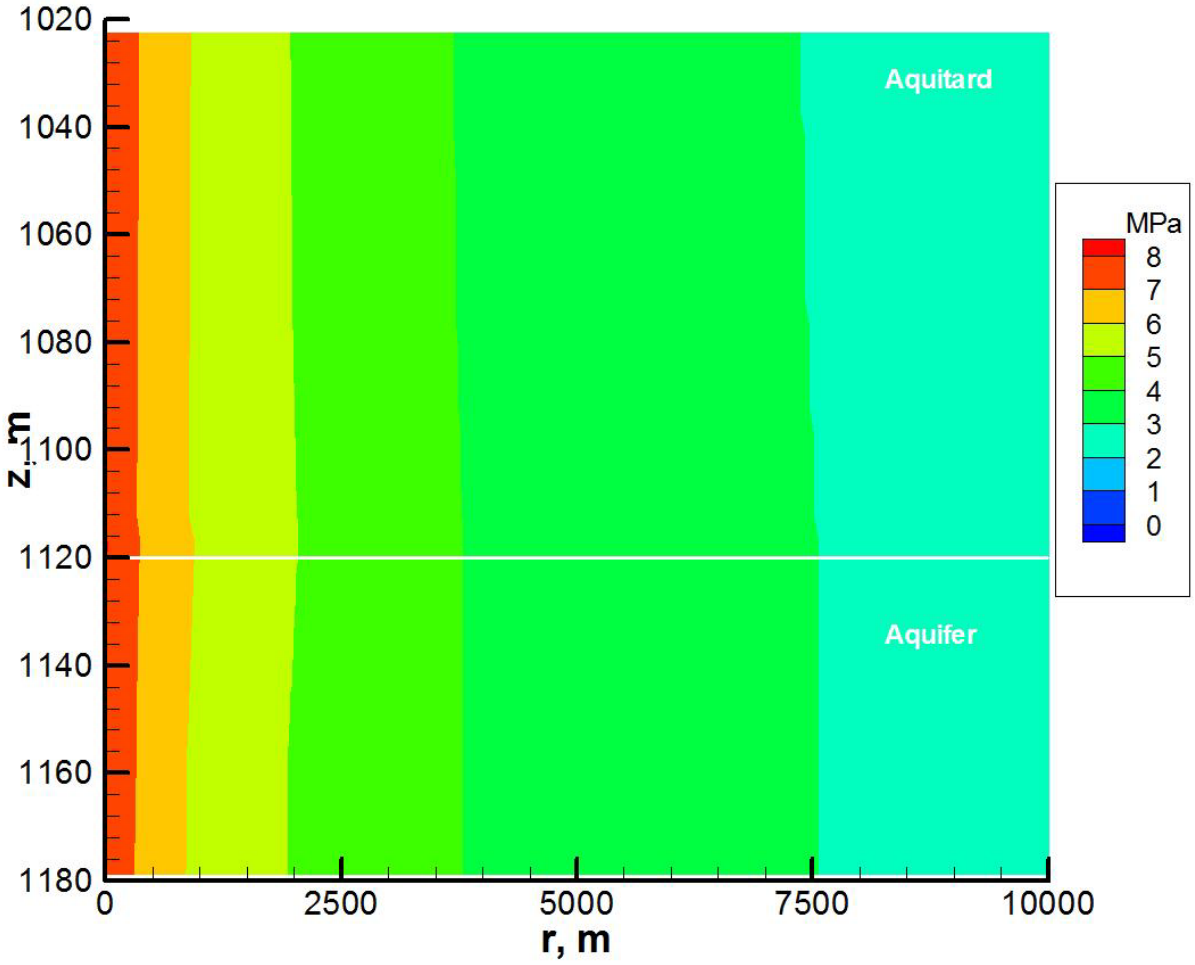

Figure 7: Pressure buildup, MPa, at 30 years injection; modified Birkholzer et al. (2008) simulation with constant permeability and porosity.

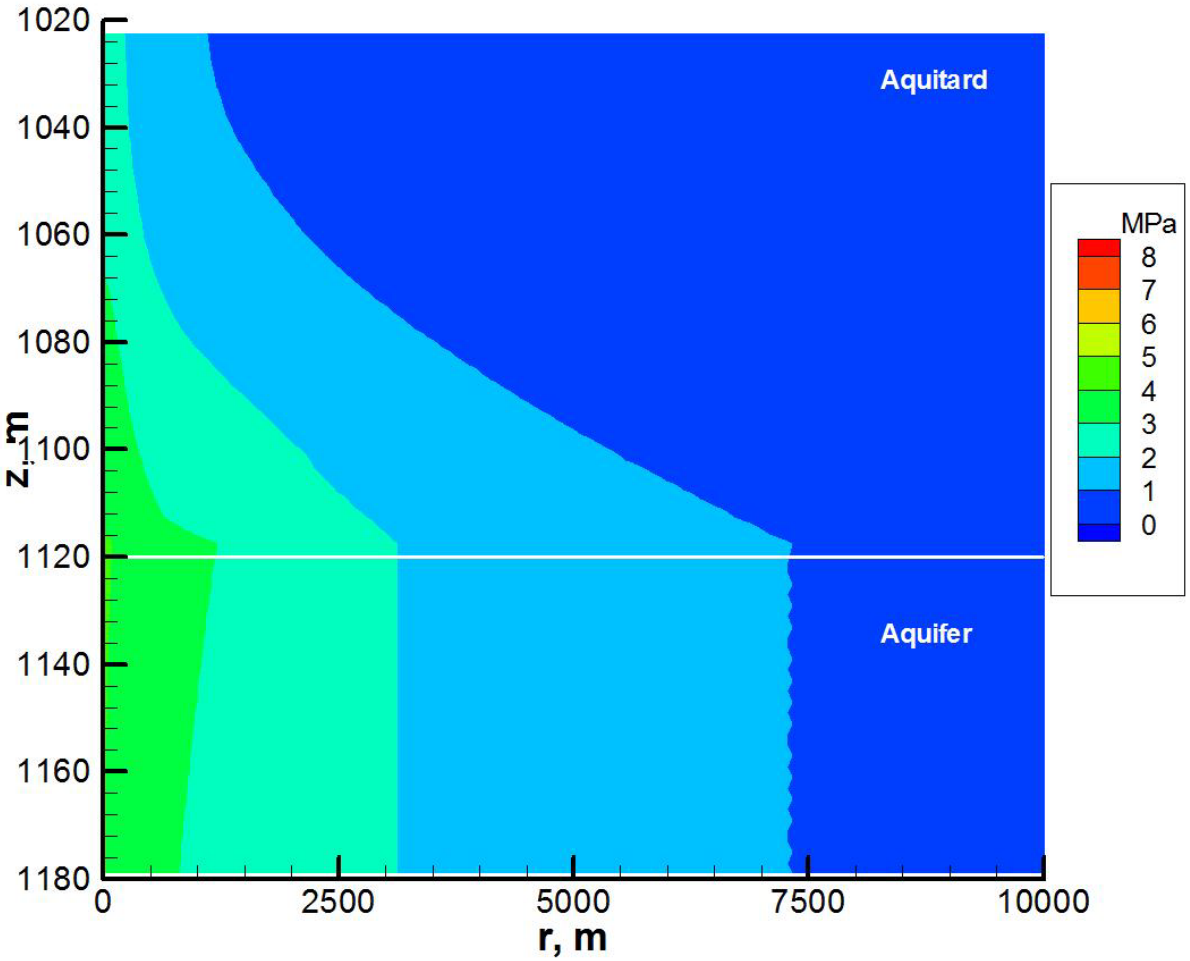

Figure 8: Pressure buildup, MPa, at 30 years injection; modified Birkholzer et al. (2008) simulation with Porosity Option 2 from Table 1 and Permeability Option 1 from Table 2.

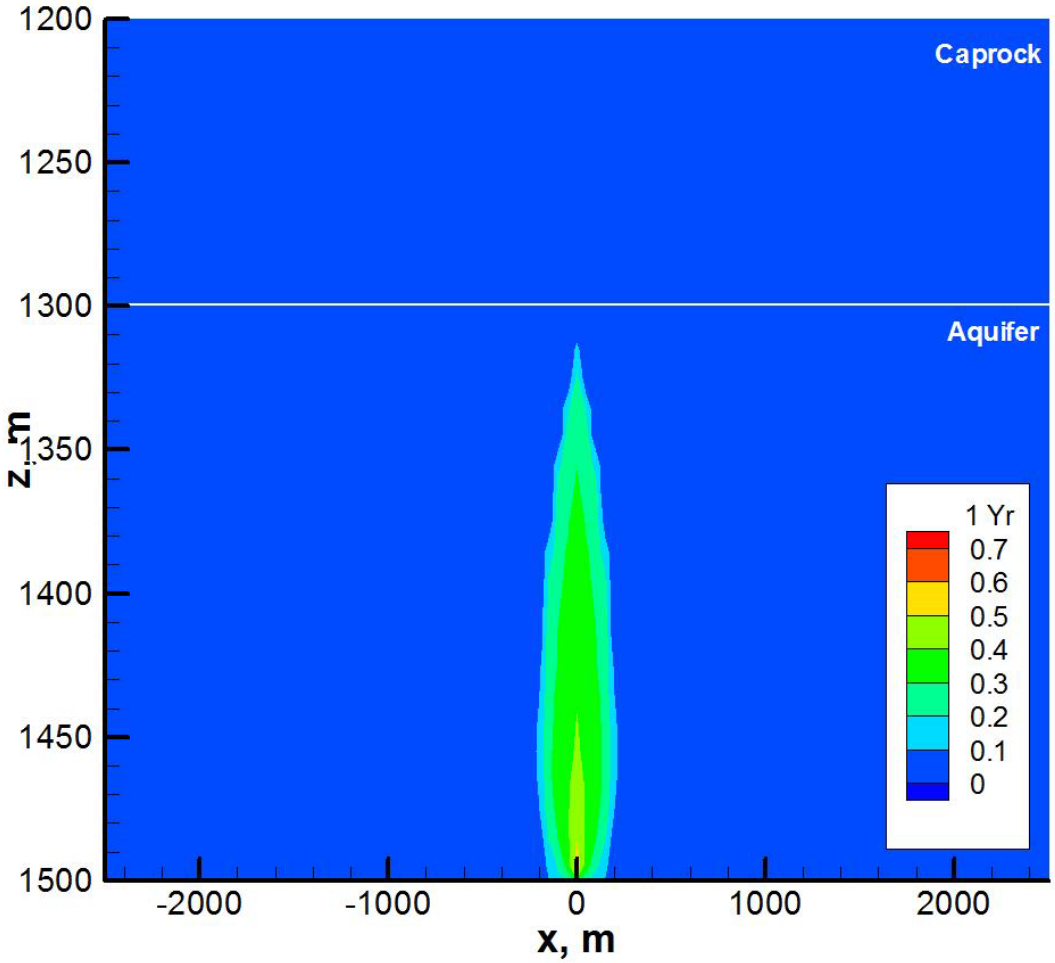

Figure 9: CO_2 saturation profile at 1 year; modified Rutqvist and Tsang (2002) simulation with Porosity Option 1 from Table 1 and Permeability Option 1 from Table 2.

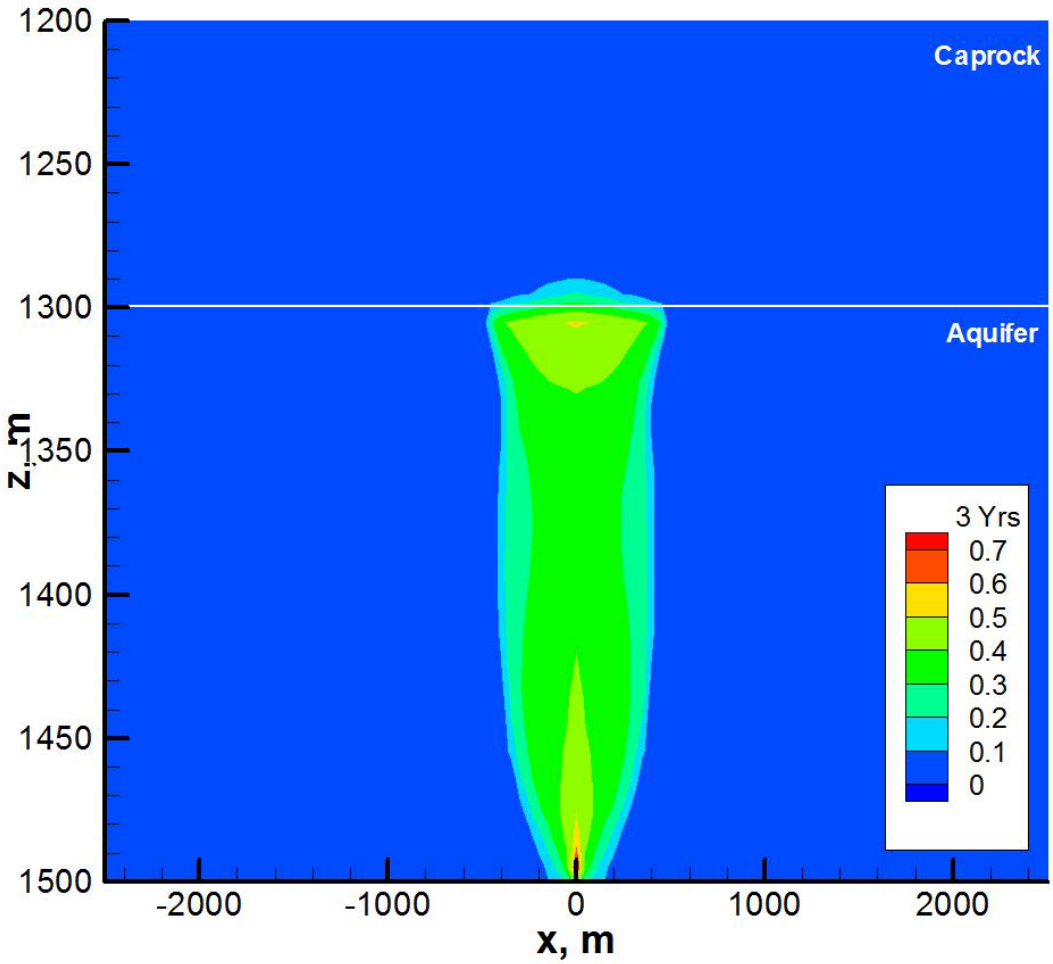

Figure 10: CO_2 saturation profile at 3 years; modified Rutqvist and Tsang (2002) simulation with Porosity Option 1 from Table 1 and Permeability Option 1 from Table 2.

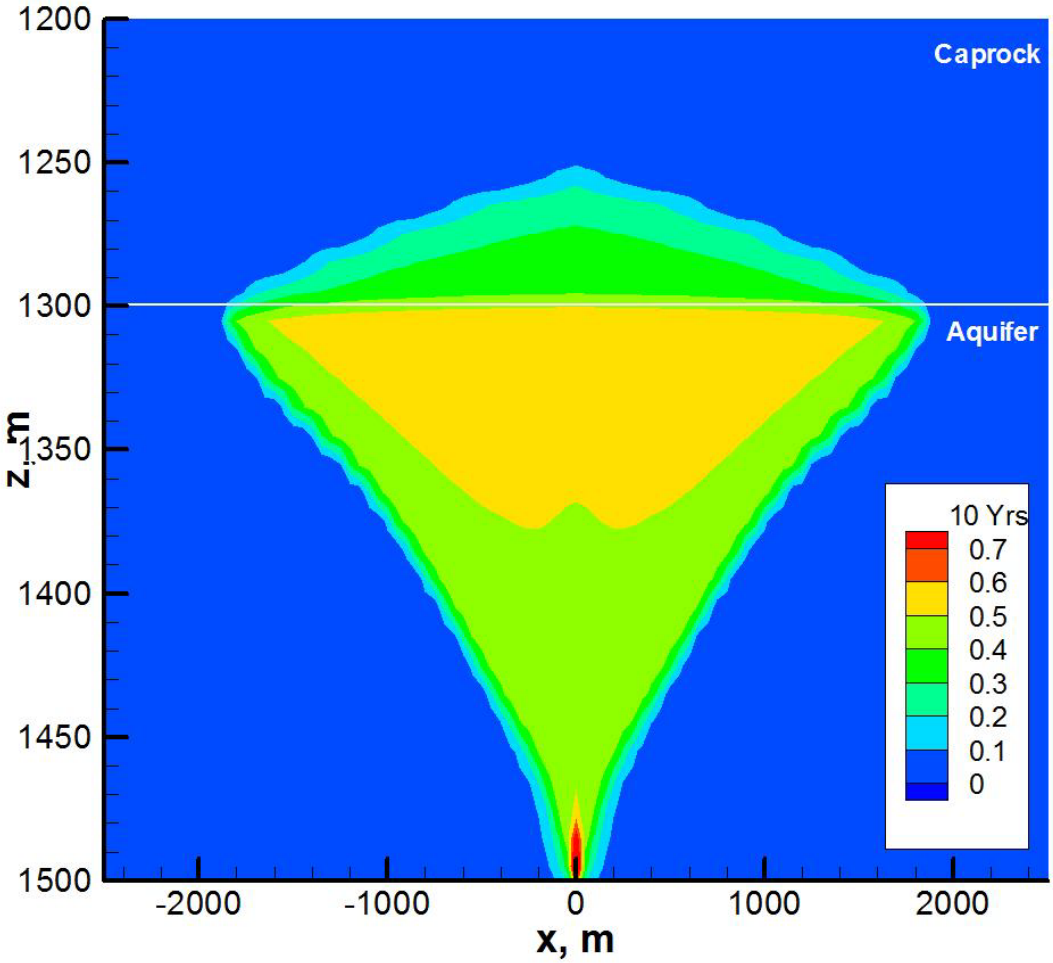

Figure 11: CO_2 saturation profile at 10 years; modified Rutqvist and Tsang (2002) simulation with Porosity Option 1 from Table 1 and Permeability Option 1 from Table 2.

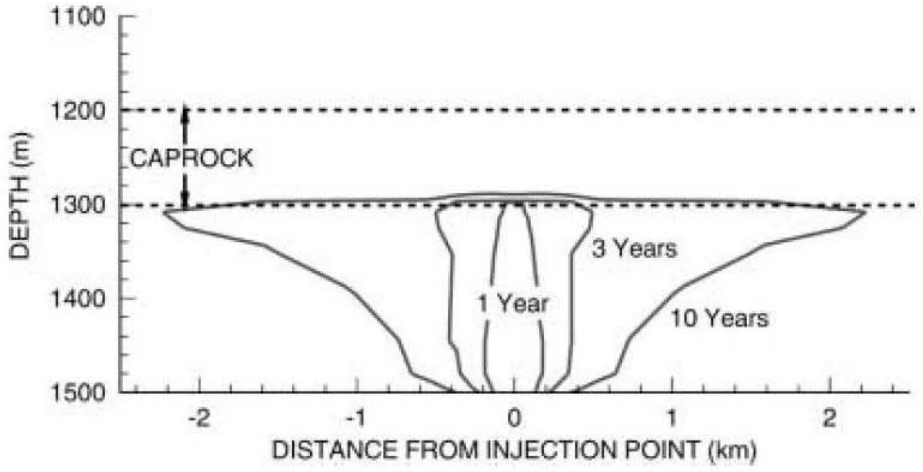

Figure 12: Rutqvist and Tsang (2002) CO_2 saturation profile at 1, 3, and 10 years.

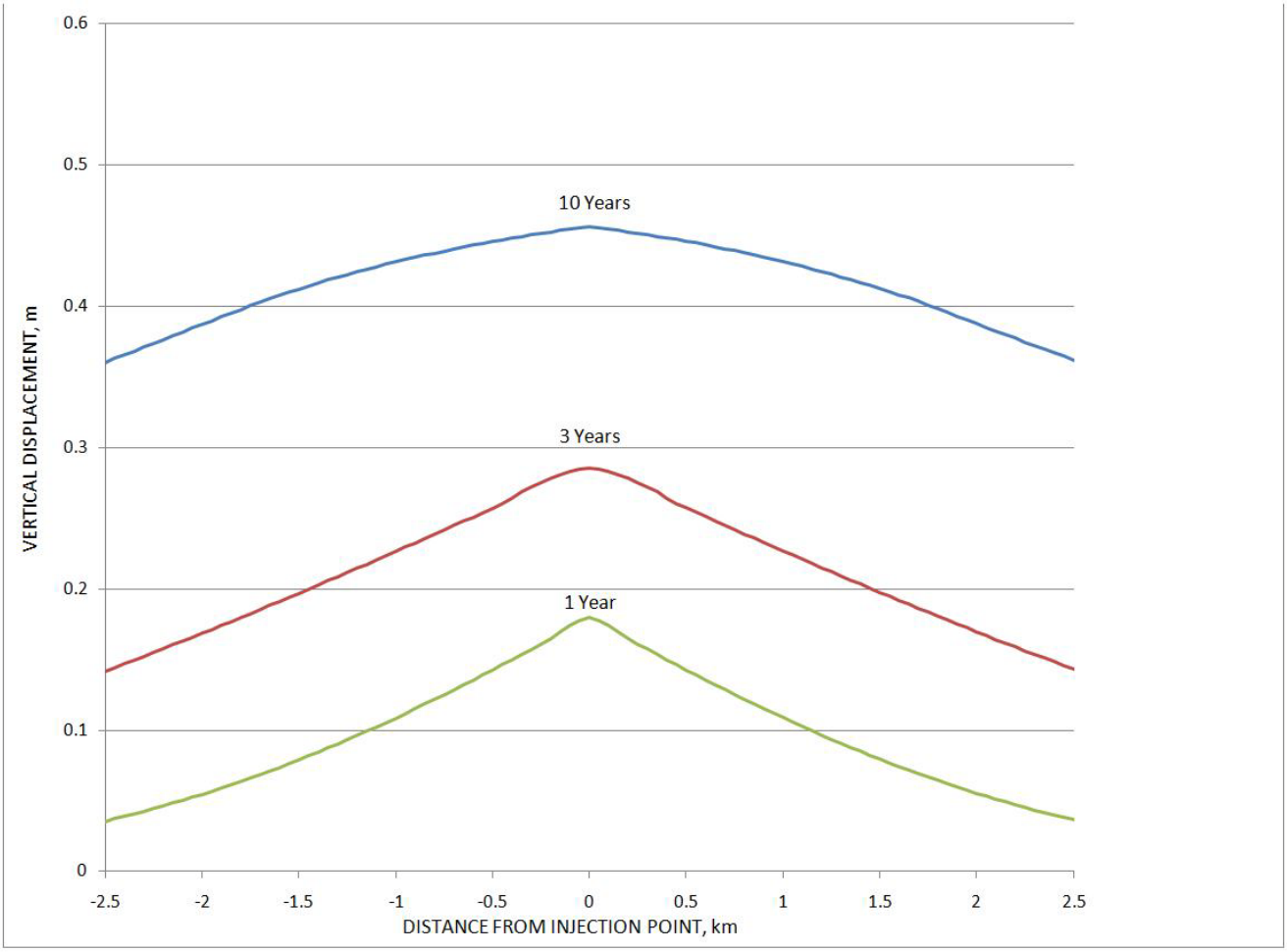

Figure 13: Surface uplift at 1, 3, and 10 years; modified Rutqvist and Tsang (2002) simulation with Porosity Option 1 from Table 1 and Permeability Option 1 from Table 2.

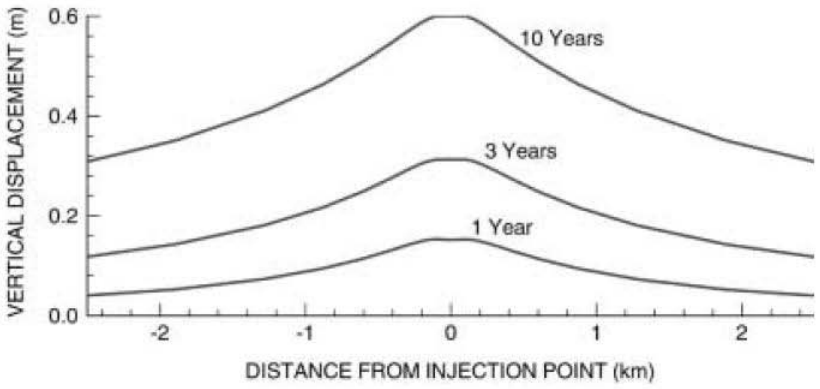

Figure 14: Rutqvist and Tsang (2002) surface uplift at 1, 3, and 10 years.

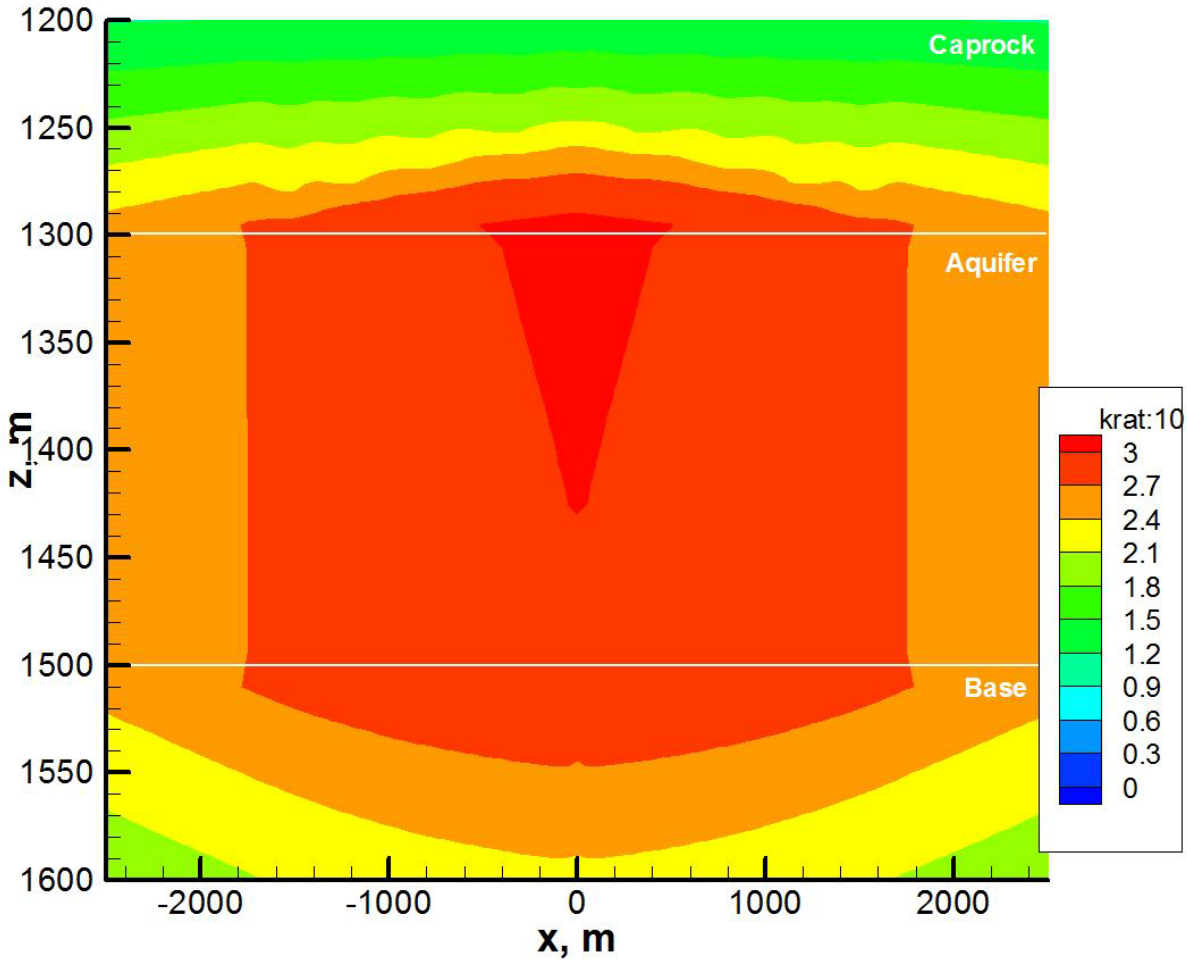

Figure 15: Permeability changes in the vicinity of the injector; modified Rutqvist and Tsang (2002) simulation with Porosity Option 1 from Table 1 and Permeability Option 1 from Table 2.

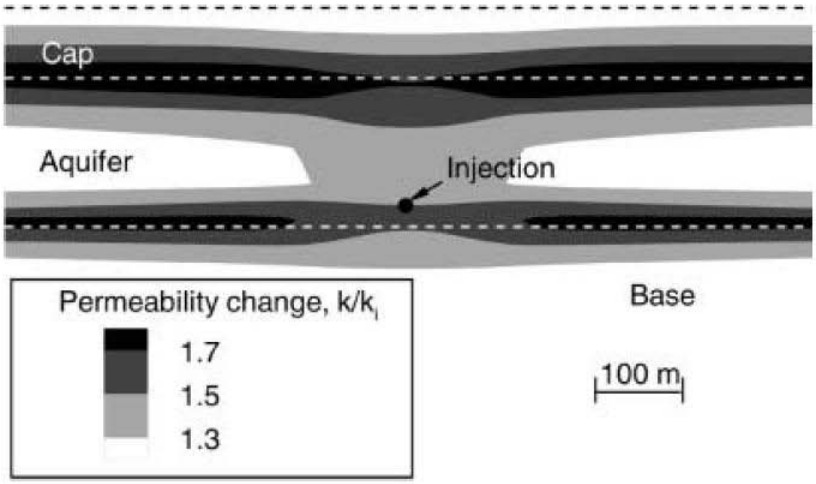

Figure 16: Rutqvist and Tsang (2002) permeability changes in the vicinity of the injector.

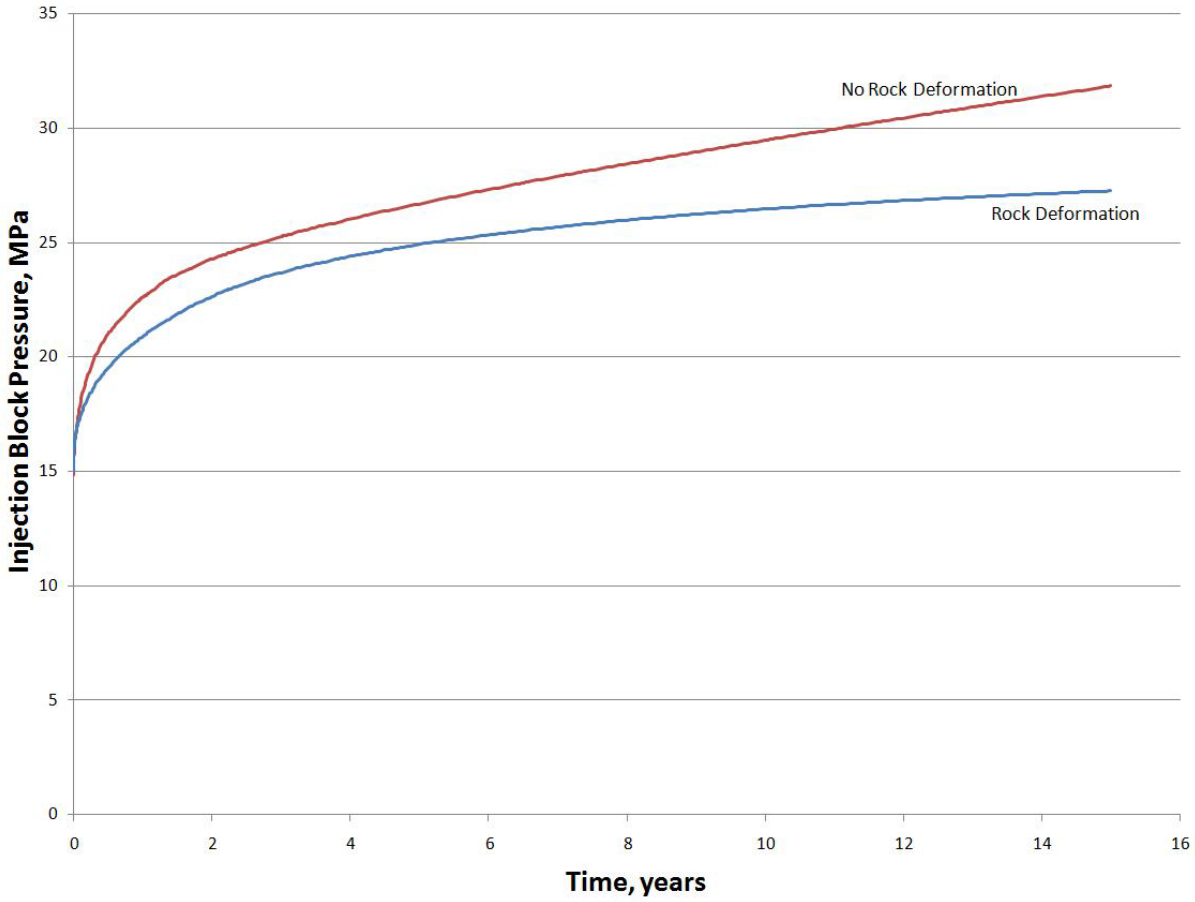

Figure 17: Comparison of injection block pressures of modified Rutqvist and Tsang (2002) simulation with and without rock deformation.

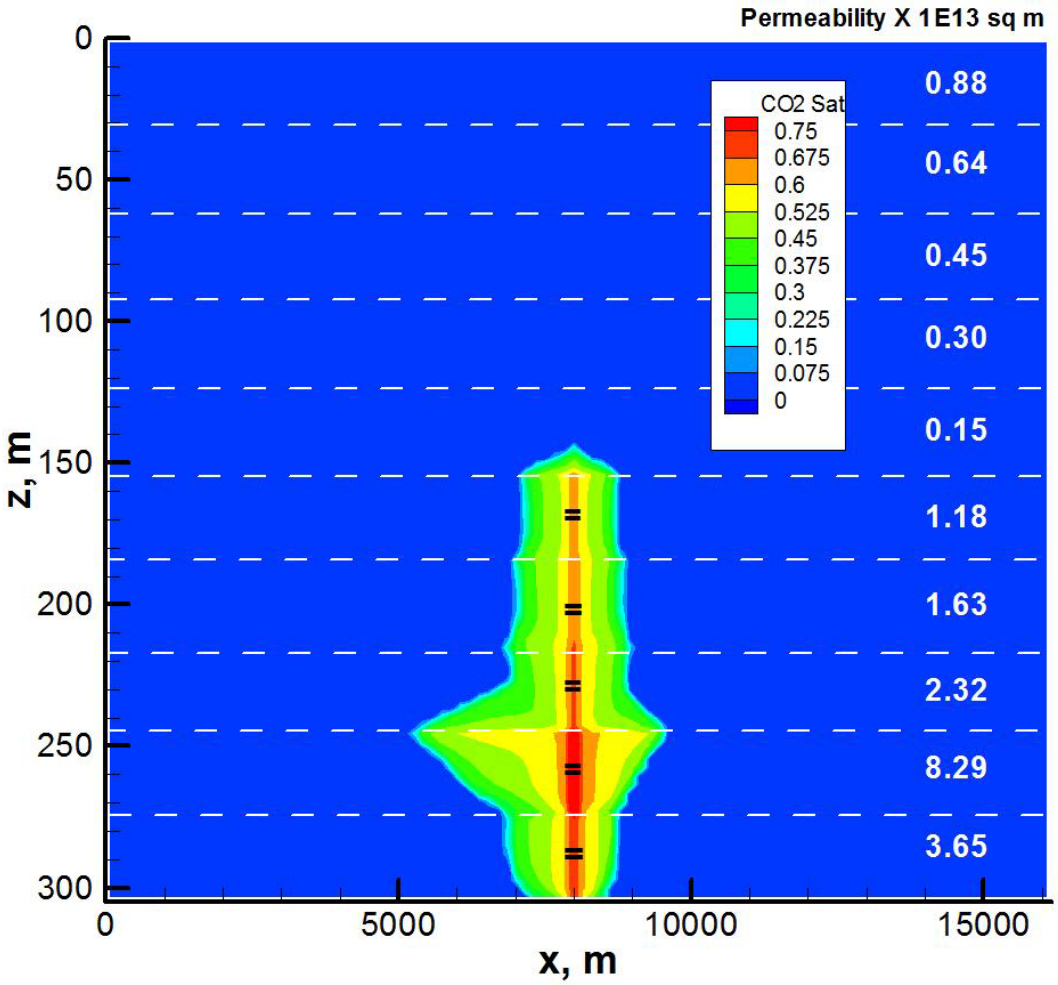

Figure 18: CO_2 saturation profile after 50 years of injection for cross section containing injection well; modified Kumar et al. (2005) simulation with finer grid.

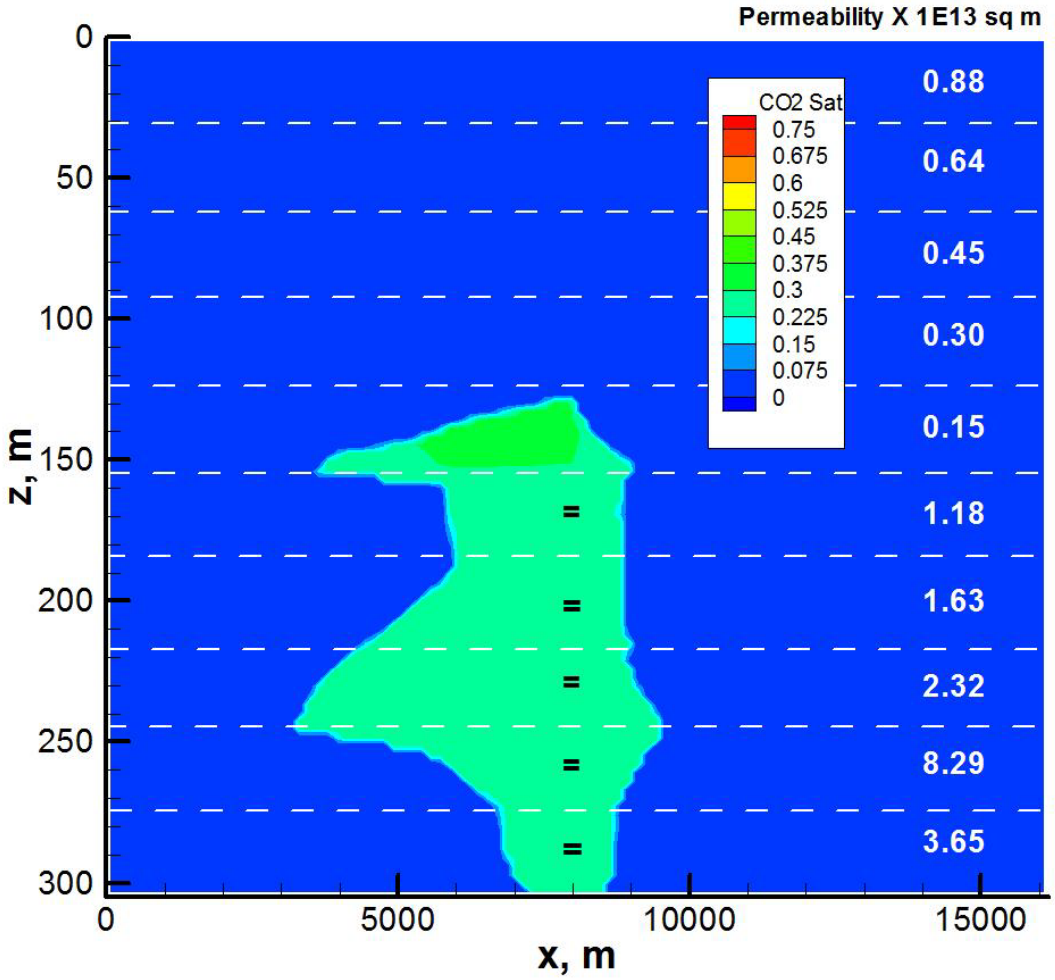

Figure 19: CO_2 saturation profile after 1,000 years for cross section containing injection well; modified Kumar et al. (2005) simulation with finer grid.